



# Performance of five high resolution satellite-based precipitation products in arid region of Egypt: An evaluation

Mohamed Salem Nashwan<sup>a,b,\*</sup>, Shamsuddin Shahid<sup>b</sup>, Ashraf Dewan<sup>c</sup>, Tarmizi Ismail<sup>b</sup>, Noraliani Alias<sup>b</sup>

<sup>a</sup> Department of Construction and Building Engineering, College of Engineering and Technology, Arab Academy for Science, Technology and Maritime Transport (AASTMT), 2033 Elhorria, Cairo, Egypt

<sup>b</sup> Department of Hydraulics and Hydrology, School of Civil Engineering, Faculty of Engineering, Universiti Teknologi Malaysia (UTM), 81310 Skudai, Johor, Malaysia

<sup>c</sup> Spatial Sciences Discipline, School of Earth and Planetary Sciences, Curtin University, Perth, Australia

## ARTICLE INFO

### Keywords:

GSMaP  
CHIRPS  
PERSIANN  
ARC  
TAMSAT  
Egypt  
Rainfall  
Remote Sensing

## ABSTRACT

High-resolution daily precipitation estimation is very important in climatological and meteorological studies in the arid regions of the world, as precipitation events in these areas can be sporadic, localized and of very high intensity. In this study, the daily performance of five, ARC2, CHIRPS v2.0, GSMaP (v. 6), TAMSAT (v. 3) and PERSIANN-CCS high resolution satellite-based gauge-corrected precipitation products were compared, and the individual performances validated against rain gauge station records in the arid region of Egypt. Seven statistical metrics (three continuous and four categorical), and selected intensity categories, were employed in the modelling of rainfall totals for the 2003 to 2018 period. In general, the results indicated poor outcomes for all the satellite-based products. CHIRPS was best at estimating rainfall of < 1 mm/day; this represented 30% of wet days during the study period. ARC and GSMaP performed better in estimating rainfall events with an intensity category of  $\geq 1$  mm/day, however both produced a high number of false detections. Despite continuous improvement of TAMSAT, it recorded the worst performance among the products evaluated. The study concluded that GSMaP appeared to be the “best” to use for supporting research activities over the arid Egyptian domain given its performance relative to the other satellite-based precipitation products.

## 1. Introduction

Accurate measurement of the spatial and temporal distribution of rainfall is essential for a variety of socio-economic activities. Precipitation data from gauge records is still the most useful and reliable method for characterizing rainfall amount and intensity (Dewan et al., 2019; Huffman et al., 2001; Petersen et al., 2005), but these measuring stations are usually sparse and unevenly distributed, and therefore cannot provide sufficient detail about the distribution of rainfall (Nashwan et al., 2019; Salman et al., 2019). Due to this issue, several satellite-based rainfall products have recently emerged as alternative sources. These are regarded as an important data source due to the high satellite coverage across the globe. They have been widely used in various hydro-climatological, and meteorological studies in various parts of the world where continuous gauge records are scarce, and/or not available at all (Abdel-Fattah et al., 2017; Mashaly and Ghoneim, 2018). In general, satellite-based rainfall estimates are

obtained through the use of Thermal Infrared Radiation (TIR), or passive microwave channels (Levizzani and Cattani, 2019). Algorithms are used for the indirect estimation of rainfall from the cloud top brightness temperature extracted from the TIR images. Due to this indirect measurement method and the attendant high likelihood of misclassification of rain-producing clouds, some uncertainty exists regarding the accuracy of the final results (Trejo et al., 2016). Even though passive microwave sensors, which are mounted on low earth-orbiting satellites, directly measure the atmospheric liquid water content, and appear to provide relatively more accurate estimates of precipitation, their temporal measurement is low. To overcome issues associated with the common indirect and microwave methods currently used in estimating rainfall, the use of TIR, microwave radiometer data coupled with numerical models and/or ground observation is currently believed to have very good potential for spatiotemporal estimate of rainfall (Ushio et al., 2009).

Egypt, which is located within an arid climatic zone, is highly

\* Corresponding author at: Department of Construction and Building Engineering, College of Engineering and Technology, Arab Academy for Science, Technology and Maritime Transport (AASTMT), 2033 Elhorria, Cairo, Egypt.

E-mail address: [s.mohamed@graduate.utm.my](mailto:s.mohamed@graduate.utm.my) (M.S. Nashwan).

<https://doi.org/10.1016/j.atmosres.2019.104809>

Received 7 October 2019; Received in revised form 8 December 2019; Accepted 19 December 2019

Available online 20 December 2019

0169-8095/ © 2019 Elsevier B.V. All rights reserved.

dependent on the Nile River for its water supply (Stanley and Warne, 1993). This water is vital for the country's economy. The recent construction and commissioning of the Ethiopian Grand Renaissance Dam is likely to adversely affect the amount of water Egypt can obtain from the Nile, and serious concerns have been raised regarding possible ongoing future water shortages (Hamed, 2019; Nashwan and Shahid, 2019a). As a result of these concerns regarding water security, the utilization of rainfall as a secondary source of water has gained increasing attention in recent years (Abdel-Shafy et al., 2010; Gado and El-Agha, 2019). Rainfall has always been the prime source of freshwater for many agricultural communities and the nomadic Bedouin, especially in the coastal north and east of Egypt (Cole and Altorki, 1998). Unfortunately, the cost of setting up a dense network of gauging stations or radar systems to provide adequate operational data to use for implementing possible rainfall-based water conservation strategies has been a serious obstacle in Egypt, as it has for many emerging economies (Nikolopoulos et al., 2013). Given this issue, the use of satellite data to provide fine resolution measurements of rainfall has shown great promise for use in the management and conservation of water resources.

Egypt has been impacted by several catastrophic flash flood events in recent years which have led to hundreds of casualties and significant economic loss (Abuzied et al., 2016; Cools et al., 2012; El-Magd et al., 2010; El Bastawesy et al., 2009; FloodList, 2015; FloodList, 2018; Gado et al., 2019; Krichak et al., 2000; Youssef et al., 2011). Egypt is ranked 3rd in regards the total number of flash flood casualties among the Mediterranean countries between the years 1990 and 2006 (Llasat et al., 2010). Studies have revealed that intense rainfall events trigger most of the flash floods in these arid areas (Costa, 1987; Nashwan et al., 2019a). The flash floods resulting from high intensity and magnitude rainfall event over New Cairo City, on 24 April 2018 (FloodList, 2018), show that these events can be extremely localized. A nearby recording station, only 5 km from the city, received only 2 mm of total rainfall on that day (OGIMET, 2018). High spatial resolution rainfall data is, therefore, a viable alternative which can capture localized extreme rainfall events which have the capacity to produce flash floods at the local level (Smith and Rodriguez, 2017). The ability to acquire bias-free estimates of rainfall is expected to significantly improve the observational capabilities of flood warning systems, particularly for these flash flood events. Reliable, high-resolution rainfall estimation techniques are required to allow Egyptian authorities to design and implement mitigation measures to counter future water-stress scenarios and hydro-meteorological disasters (Abutaleb et al., 2018; Nashwan et al., 2018a; Nashwan et al., 2019c).

Significant efforts have recently been made to produce high spatial resolution (i.e.  $0.1^\circ$  or higher) satellite-based global, or regional, rainfall products (Gella, 2019). In 2004, the Center for Hydrometeorology and Remote Sensing at the University of California, Irvine, developed a Precipitation Estimation from Remotely Sensed Information using Artificial Neural Networks-Cloud Classification System (PERSIANN-CCS) technique. This has a spatial resolution of  $0.04^\circ \times 0.04^\circ$ , and provides half-hourly temporal coverage (Hong et al., 2004). The US Climate Prediction Center (CPC) released their second version of the African Rainfall Climatology (ARC) in 2012 that provides daily estimates of rainfall over Africa at a  $0.1^\circ \times 0.1^\circ$  spatial grid (Novella and Thiaw, 2013). In 2014, the Japan Science and Technology Agency (JST) and the Japanese Aerospace Exploration Agency (JAXA), developed the  $0.1^\circ$ /hourly Global Satellite Mapping of Precipitation (GSMaP) dataset for global precipitation (Ushio et al., 2009). The Climate Hazard Group released the  $0.05^\circ$  resolution InfraRed Precipitation with Stations (CHIRPS) in 2015 for supporting quasi-daily global estimate of rainfall (Funk et al., 2015). Recently, University of Reading released their latest version of the Tropical Applications of Meteorology using SATellite data and ground-based observations (TAMSAT v. 3), which provides  $0.0375^\circ$ /daily rainfall over Africa (Maidment et al., 2017). Owing to uncertainties commonly associated with satellite-based estimation, a rigorous evaluation of the products is necessary to increase the level of

confidence in their use in different areas of application.

The performances of the ARC2, CHIRPS v.2.0, GSMaP (v. 6), PERSIANN-CCS and TAMSAT (v. 3) products have been evaluated by determining their ability to estimate precipitation in the different regions or countries in Africa (Bayissa et al., 2017; Cattani et al., 2018; Dembélé and Zwart, 2016; Fenta et al., 2018; Gella, 2019; Trejo et al., 2016). Recently, Nashwan et al. (2019d) investigated the performance of GSMaP (v. 7), CHIRPS v2.0 and the IMERG over Egypt for the period of 2014–2018, and observed that CHIRPS is better at estimating the total amount of rainfall. However, CHIRPS did tend to overestimate rainfall occurrences. Furthermore, Nashwan and Shahid (2019b) compared the performance of CHIRPS with six widely used, gauge-based, gridded rainfall datasets for the period 1979–2014. They found that CHIRPS recorded the highest amount of erroneous estimates at the monthly scale among the gauge-based, gridded, precipitation datasets. El Kenawy et al. (2019) reported that the PERSIANN-Climate Data Record (CDR) failed in reproducing extreme wet days in the Middle East. Little is known about the accuracy of either ARC2, GSMaP (v. 6), PERSIANN-CCS or TAMSAT (v. 3) over Egypt. A number of studies, however, have been conducted to assess the performance of the different, satellite-based precipitation products in nearby countries with a similar climate. Dinku et al. (2010) found that GSMaP (v. 5) and ARC (v. 1) overestimated rainfall occurrence over North Africa. CHIRPS is found to overestimate rainfall over Cyprus (Katsanos et al., 2016). GSMaP (v. 6) showed good correlation but underestimated rainfall over Antalya, Turkey (Saber and Yilmaz, 2018). Dembélé and Zwart (2016), reported poor performance of CHIRPS and ARC over semi-arid regions of Burkina Faso. Furthermore, Babaousmail et al. (2019), noted that CHIRPS performed poorly at the daily scale over arid Algeria. Basheer and Elagib (2019), evaluated performance of ARC2, CHIRPS v2.0, TAMSAT (v. 2) over semi-arid and sub-humid South Sudan, and reported a good performance of CHIRPS at monthly and annual scales. There is a lack of detailed knowledge regarding the reliability of the ARC2, CHIRPS v2.0, GSMaP (v. 6), PERSIANN-CCS and TAMSAT (v. 3) products, especially over arid regions of Egypt.

This study evaluates the performance of five freely available, high spatial resolution, satellite-based precipitation products over the hot desert climate of Egypt. Another product currently available, the Integrated Multi-satellite Retrievals for GPM (IMERG) dataset, was not included in this study due to its relatively short temporal pass over Egypt (Nashwan et al., 2019d).

## 2. Study area, data and review of literature

### 2.1. Study area

Located in the northeast of the African continent, Egypt covers an area of nearly one million square kilometers. Most of the topography is relatively flat, with elevations ranging from 0 to 300 m above mean sea level (Fig. 1). The Nile River enters Egypt from the south and flows in a northerly direction, dividing the country into Western and Eastern deserts. Due to the fertility of the river soils, much of the country's population is located along the banks, and within the deltaic plain, of the Nile River (Abdallah, 2017; CAPMAS, 2019; Nashwan et al., 2019b).

The climate of Egypt is classified as hot desert arid type. Rainfall occurs mainly in winter (NDJF), with the wettest month being January (with an average rainfall of 120 mm) (Nashwan and Shahid, 2019b). Fig. 1 shows the spatial distribution of rainfall in Egypt, with the wettest coastal regions located to the north and east. The inland south and west are the driest parts of the country.

### 2.2. Data

The current study has evaluated the performance of five satellite-based precipitation datasets and has used daily ground observations of rainfall as a reference. A brief description of the different datasets is

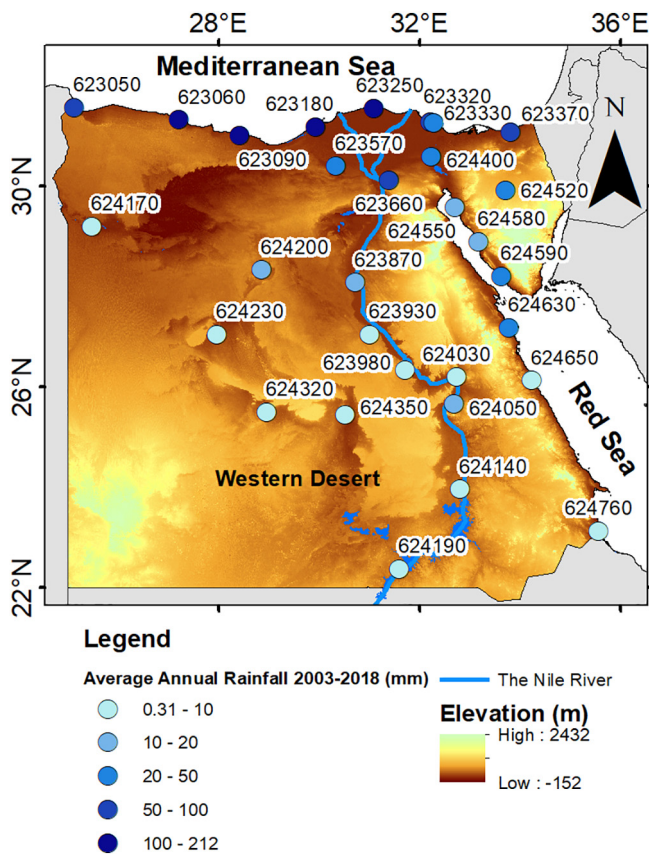


Fig. 1. Elevation of Egypt. Rain gauge locations have been overlain on the elevation data. Average annual rainfall at each location is symbolized with the relevant colour code.

given below.

2.2.1. Ground observations

The daily rainfall data from 30 gauging stations was obtained from the US National Climate Data Center Global Summary of Days (GSOD) database, for the period January 2003 to December 2018. The gauges are located across Egypt, as shown in Fig. 1. The count of wet days, the maximum recorded rainfall amount (mm/day), and the percentage of missing data within the study period for each station, is presented in Table 1. The individual locations were verified using the WMO Integrated Global Observing System (WIGOS) dataset.

Table 1

The number of wet days, maximum daily rainfall (mm/day) and percentage of missing record during 2003–2019 period for each station.

WMO ID	Wet days	Max daily rainfall (mm)	% of missing record	WMO ID	Wet days	Max daily rainfall (mm)	% of missing record
623050	214	70.10	15%	624140	12	14.99	2%
623060	478	99.06	1%	624170	32	11.94	2%
623090	471	99.06	4%	624190	4	26.16	36%
623180	566	252.22	1%	624200	12	102.11	1%
623250	463	71.88	17%	624230	10	24.89	4%
623320	243	90.93	35%	624320	3	72.14	17%
623330	261	90.93	2%	624350	4	2.03	1%
623370	300	80.01	5%	624400	125	101.09	22%
623570	95	99.06	29%	624520	93	102.11	4%
623660	170	106.17	1%	624550	92	86.11	2%
623870	23	76.20	1%	624580	73	19.05	2%
623930	12	9.91	1%	624590	43	99.06	3%
623980	1	7.87	22%*	624630	24	102.11	1%
624030	16	7.11	20%	624650	8	6.10	5%
624050	28	50.04	1%	624760	11	35.05	27%

WMO ID: World Meteorological Organization Identification number; \*: Percentage of missing records for the station 623980 was calculated from its starting day (16 May 2013).

Table 2

Contingency table presents agreement between observed records (Po) and satellite-based retrievals (Ps) of rainfall for different rainfall intensity ranges.

	Po ≥ Threshold	Po < Threshold
Ps ≥ Threshold	Hits	False Alarms
Ps < Threshold	Misses	Correct Negatives

Table 3

Rainfall intensity categories.

Daily rainfall intensity category	Definition
No/tiny rainfall	$P < 1 \text{ mm}$
Light rainfall	$1 \text{ mm} \leq P < 5 \text{ mm}$
Moderate rainfall	$5 \text{ mm} \leq P < 10 \text{ mm}$
Heavy rainfall	$P \geq 10 \text{ mm}$

2.2.2. Satellite-based daily precipitation datasets

The ARC2 has been developed by NOAA CPC by integrating 3-hourly IR data recorded by the meteorological satellites of the European organization and the daily records of nearly 1200 ground stations from the GTS gauge network in Africa (Novella and Thiaw, 2013). It provides daily rainfall estimate at a 0.1° spatial resolution since 1983 but is confined only to Africa. Three main steps are used to develop this product. First, a fixed rainfall amount of 3 mm/h is assumed in areas where the cloud-top temperature is < 235 Kelvin. This assumption is then weighted, using a maximum likelihood approach, toward the nearest ground observation. Finally, the weighted rainfall estimates are integrated with ground observations, where any spatial variability is taken primarily from the satellite retrievals and the amounts of rainfall determined from the ground observations. The ARC data is available at <ftp://ftp.cpc.ncep.noaa.gov/fews/fewsdata/africa/arc2>

CHIRPS v2.0 is produced by the US Geological Survey and the Climate Hazards Group (CHG) at the University of California, Santa Barbara. This product collates data from five sources and uses a four-step development process: (1) a 5-day (pentad) precipitation estimate is generated from the 3-hourly quasi-global geostationary TIR data of CPC and the National Climatic Data Center; (2) a TRMM multi-satellite precipitation analysis (TMPA)-3B42 rainfall product is used to calibrate the IR pentad estimate; (3) the calibrated IR pentad product is then multiplied with the Climate Hazards Precipitation Climatology and subsequently divided by the long-term mean to produce the CHG IR Precipitation (CHIRP) data; and finally, (4) model precipitation data from NOAA Climate Forecast System are used to provide CHIRP with daily variability, and ground-based observations are used to correct for

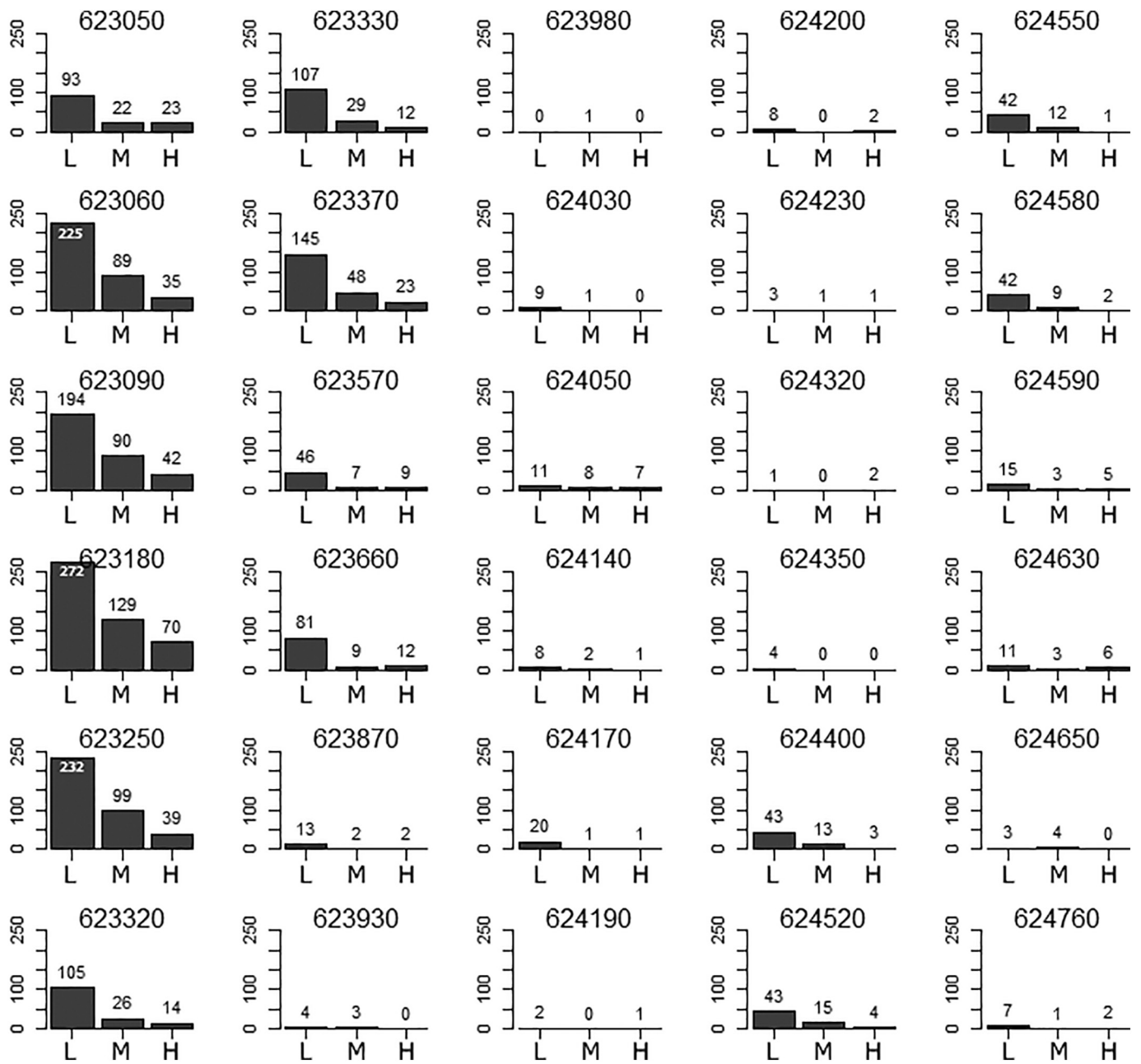


Fig. 2. Bar graphs, showing the number of rainy days within the light (L), moderate (M) and heavy (H) rainfall intensity categories for each station.

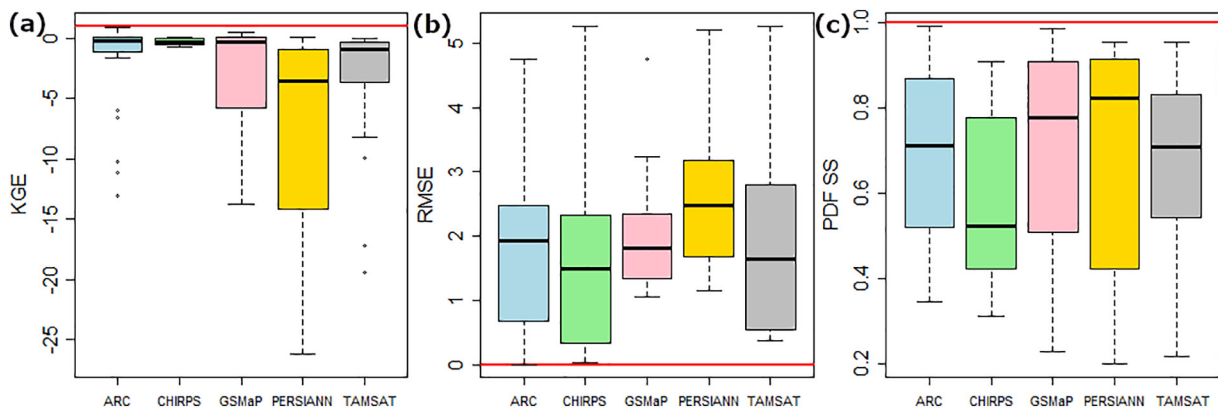


Fig. 3. The box and whisker plots of: (a) KGE, (b) RMSE, and (c) PDF SS estimated for different satellite-based rainfall products. Each box plot represents an evaluation of 30 gauge stations. The horizontal red lines are the optimal value of each metrics.

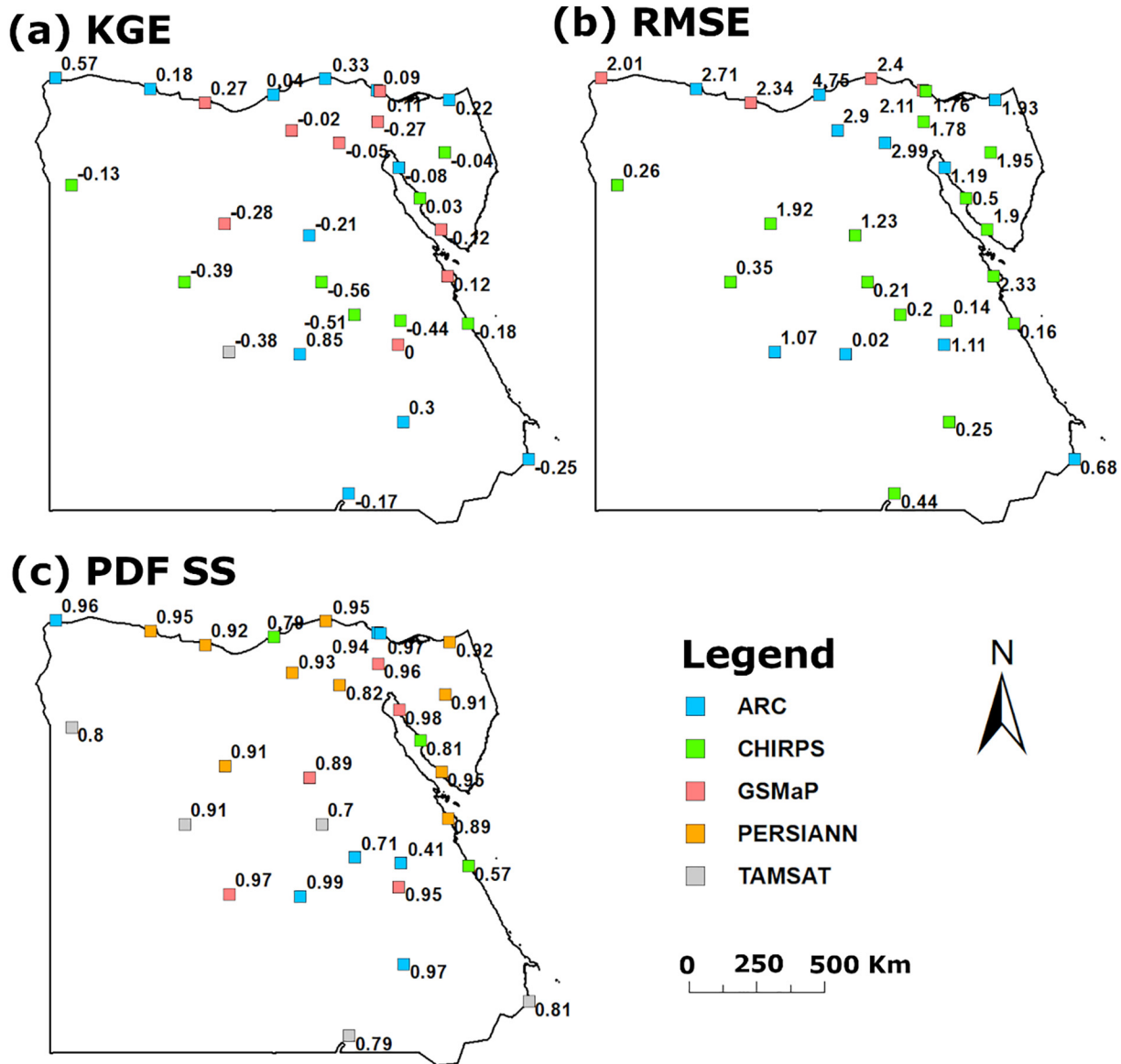


Fig. 4. Spatial distribution of the results denoting the best performing satellite-based rainfall product at each gauge station according to: (a) KGE, (b) RMSE and (c) PDF SS. (For interpretation of the references to colour in this figure legend, the reader is referred to the web version of this article.)

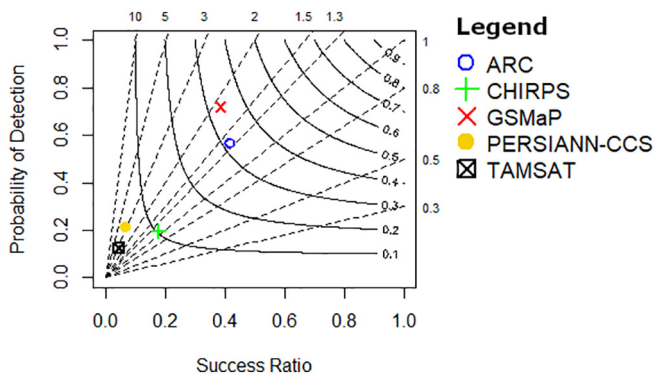


Fig. 5. Performance diagram summarizing the results of POD, SR, Hit BIAS, and CSI of the five products.

monthly climatology of the final product. This product provides near-global daily rainfall data since 1981 at a 0.05° spatial grid.

GSMaP has been developed by JST and JAXA. It combines several

Passive Microwave (PMW) and IR sensor data to produce 0.1° resolution satellite-based precipitation product. The GSMaP algorithm uses several steps when processing data. They are: (1) the PMW radiometer retrievals, based on different satellite platforms, provide an instantaneous precipitation rate (Aonashi et al., 2009); (2) the PMW retrievals are propagated using the cloud vectors obtained from the geo-IR maps to fill the gaps between the PMW retrievals; (3) the Kalman filter and forward and backwards morphing approach are applied to reduce retrieval errors (Ushio et al., 2009); and finally, (4) the NOAA CPC gauge-based precipitation product is used to calibrate the final product (Mega et al., 2014). Although the latest version (v. 7) has been released and is available for this study, the earlier version (v. 6) was used due to the longer period of use and recorded data as compared to the latest version. This was downloaded from <https://sharaku.eorc.jaxa.jp/GSMaP/>.

TAMSAT (v. 3) has been developed by University of Reading by integrating TIR images with ground-based observations (Maidment et al., 2017). The TAMSAT algorithm is based on two assumptions: (1) rainfall is produced from convective clouds that lead to cold cloud-tops; and, (2) rainfall and the cold cloud duration (CCD, the number of hours

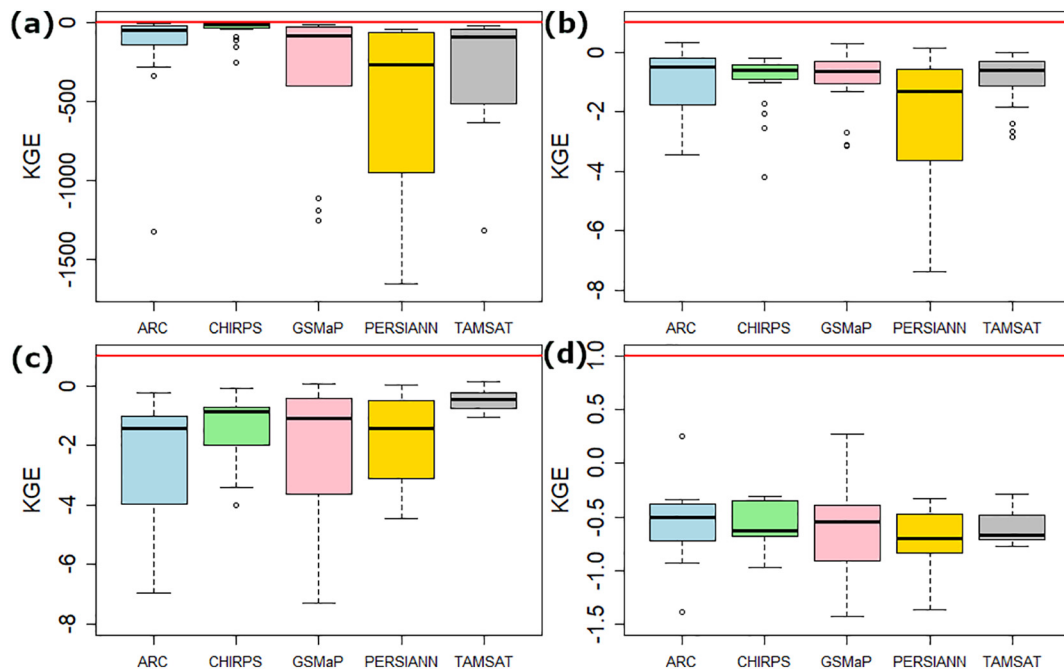


Fig. 6. The box and whisker plots of KGE estimated for the five precipitation datasets in replicating rainfall totals for: (a) no/tiny, (b) light, (c) moderate, and (d) heavy rainfall. The horizontal red lines represent the optimal KGE value.

when the brightness temperatures of TIR pixel is below a wet/dry threshold) are linearly correlated. The TAMSAT uses a spatiotemporally varying temperature threshold to calculate the CCD, which is calibrated using ground-based records. The product is an estimate of daily rainfall at a 0.0375° spatial grid and has records for Africa since 1983. This product can be accessed via <http://dx.doi.org/10.17864/1947.112>

PERSIANN-CCS extracts rainfall features from cloud coverage using different temperature thresholds. The algorithm consists of four steps: (1) incremental temperature thresholds are used to segment the infrared cloud images; (2) segmented images are then used to extract cloud features, including temperature, geometry and texture features into distinctive cloud patches; (3) the self-organizing feature map algorithm is used to cluster the cloud patches into the main categories; and (4) the relationship between brightness, temperature and rainfall rates are calibrated by histogram matching and nonlinear exponential function fitting using gauge-corrected, hourly, radar-derived rainfall data (Hong et al., 2004; Mahrooghy et al., 2012). It offers hourly and daily rainfall data with a spatial resolution of 0.04°.

### 3. Methodology

Daily ground-based rainfall observations were used to evaluate the performance of the five products, namely ARC2, CHIRPS v2.0, GSMaP (v. 6), TAMSAT (v. 3) and PERSIANN-CCS. The gauge observations at each location were compared with the nearest grid point of each satellite-based product. This approach is commonly used when assessing satellite-based precipitation products to ensure usage of their original estimates (Hobouchian et al., 2017; Rozante et al., 2018). Three continuous and four categorical, statistical metrics were used to quantify the performance of each product. The continuous metrics are the Kling–Gupta efficiency (KGE), Root Mean Square Error (RMSE) and Probability Distribution Function (PDF) and Skill Score (SS). The KGE, eq. (1), is a robust, objective metric that describes and measures overall fitness of time-series by integrating correlation, bias, and variability (Gupta et al., 2009). It ranges from  $-\infty$  with an optimal value of 1. The RMSE (eq. 2), measures standard deviation of the residuals, having an optimal value of zero. On the other hand, the PDF SS (eq. 3), measures how well the satellite-based products can capture the PDF of observed

rainfall (Perkins et al., 2007). It ranges from 0 to 1, in which 1 represents a perfect overlap between the gauge and satellite-based PDFs.

$$KGE = 1 - \sqrt{(r - 1)^2 + \left(\frac{\mu_s}{\mu_o} - 1\right)^2 + \left(\frac{\sigma_s/\mu_s}{\sigma_o/\mu_o} - 1\right)^2} \tag{1}$$

$$RMSE = \sqrt{\frac{1}{n} \sum_{i=1}^n (P_s - P_o)^2} \tag{2}$$

$$SS = \sum_{i=1}^n \min(f_s, f_o) \tag{3}$$

where,  $r$  is the Pearson's correlation;  $\mu$  and  $\sigma$  represent the mean and standard deviation of the satellite-based ( $P_s$ ) and observed ( $P_o$ ) rainfall, respectively;  $n$  is the sample size; and  $f_o$  and  $f_s$  are the frequency of a specific rainfall amount between observed and satellite-based data.

Categorical statistical metrics such as the Probability of Detection (POD), Success Ratio (SR), Critical Success Index (CSI) and the Hit BIAS (Eqs. (4)–(7)) were calculated based on a contingency table (Table 2). POD determines how well satellite-based products can capture the occurrence of ground rainfall events. The SR is the opposite of the False Alarm Ratio (FAR), which evaluates how many times a satellite-based product falsely detects rainfall events not detected by gauge records. The CSI measures the ratio of true rainy days count (estimated by both satellite-based product and ground station), to the total number of rainy days estimated by the satellite-based product. The Hit BIAS measures the number of rainy days detected by satellite-based product divided by the number of rainy days detected by the rain gauges. The POD, SR, CSI, and Hit BIAS have an optimal value of 1.

$$POD = \frac{Hits}{Hits + Misses} \tag{4}$$

$$Success\ Ratio = 1 - \frac{False\ Alarms}{Hits + False\ Alarms} \tag{5}$$

$$CSI = \frac{Hits}{Hits + Misses + False\ Alarms} \tag{6}$$

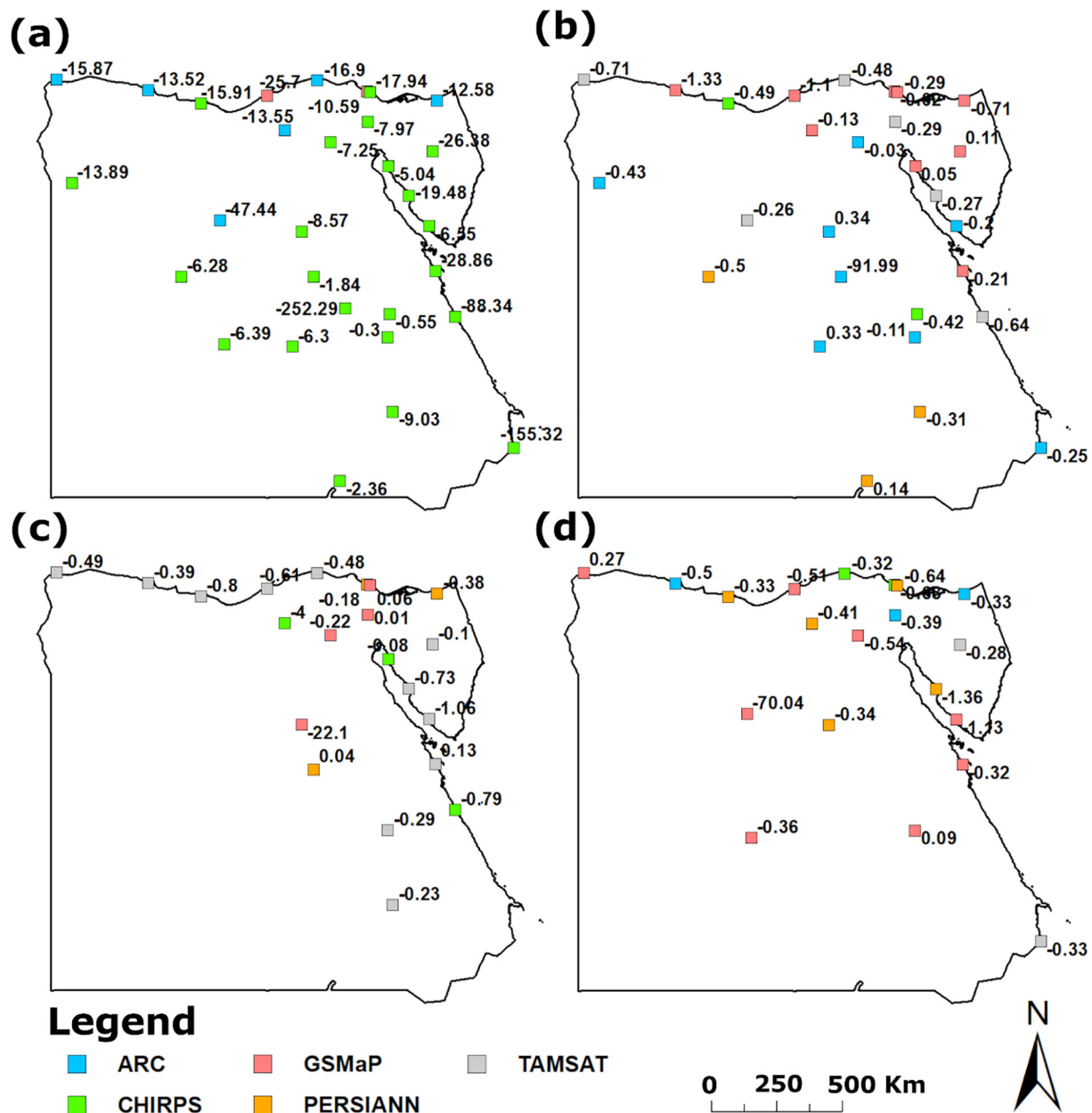


Fig. 7. Spatial distribution of the best performing satellite-based KGE precipitation products: (a) no/tiny, (b) light, (c) moderate, and (d) heavy rainfall categories. (For interpretation of the references to colour in this figure legend, the reader is referred to the web version of this article.)

$$Hit\ BIAS = \frac{Hits + False\ Alarms}{Hits + Misses} \tag{7}$$

To explore the performance of, and any errors in, the satellite-based precipitation products, daily rainfall intensity was used to categorize rainfall events based on predefined threshold values (Table 3). The thresholding definition is based on the WMO standard (WMO, 2012), with some modification to suit the arid conditions of the study area. The modification includes merging of the rainfall intensity categories > 10 mm/day. The evaluation of the satellite-based products was conducted on the complete series of rainfall and under four intensity categories (Table 3). The analysis of an intense precipitation event, which occurred on 5 February 2004, was used as a case study. Most of the gauges in Egypt recorded rainfall on that day, making it ideal for comparing gauge records using each of the five satellite-based products.

#### 4. Results

Fig. 2 shows the number of rainy days observed at different stations under light, moderate and heavy conditions. The number of days within a no/tiny rainfall category did not appear in the graphs to prevent high spikes, as this class has very high number of occurrences in Egypt, compared to other categories. In total, the ground stations recorded 153,011 days as a no/tiny rainfall class, of which 1145 were wet days with rainfall < 1 mm, 1789 were light rainfall intensity days, 627 were moderate rainfall intensity days, and 319 were heavy rainfall intensity days.

##### 4.1. Evaluation of satellite-based precipitation products for complete daily rainfall series

Fig. 3(a–c) shows the results of continuous metrics for a complete rainfall series. Fig. 4 presents maps of the best performing products at

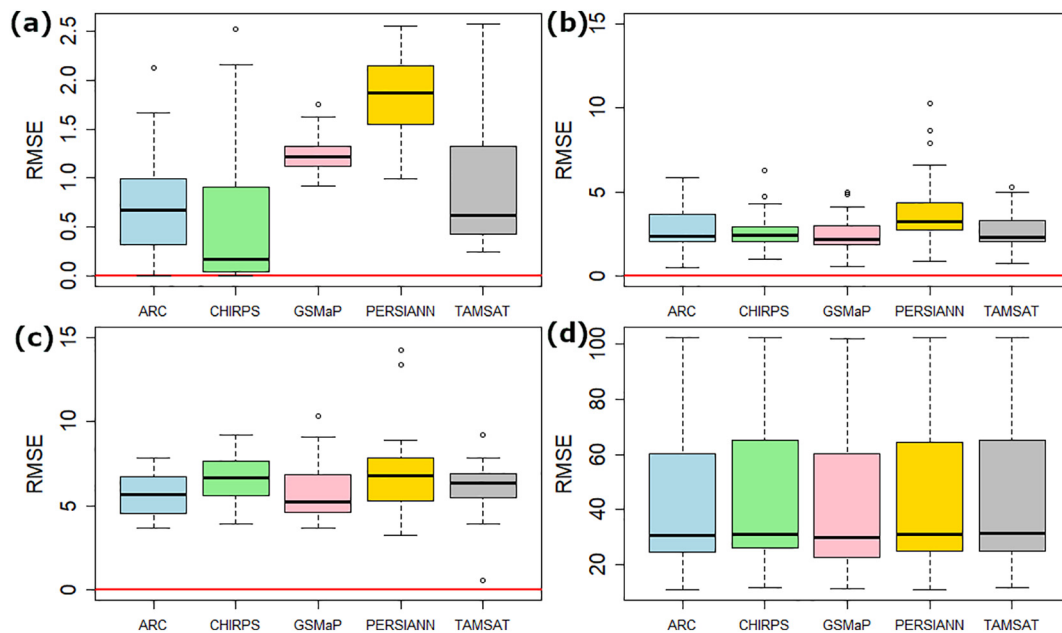


**Fig. 8.** The box and whisker plots of RMSE for the five precipitation datasets in replicating rainfall totals for: (a) no/tiny, (b) light, (c) moderate, and (d) heavy rainfall. The horizontal red lines represent the optimal RMSE value.

each station according to the four continuous metrics. Fig. 3(a) shows that ARC has a median KGE ( $-0.21$ ) nearest to the optimal KGE followed by GSMaP and CHIRPS ( $-0.28$  and  $-0.37$ , respectively). Although CHIRPS indicates the lowest range of KGE (suggesting a low spatial variability), ARC is a better performing product for many stations than CHIRPS. PERSIANN is the worst product according to the KGE. According to the RMSE value, all the products show good performance (Fig. 3(a)). CHIRPS shows the lowest RMSE with a median of 1.49 and appears to be the best product as shown by results from the majority of the stations. Although the median RMSE of ARC is lower than that of GSMaP, ARC records the best results at 10 stations, while GSMaP is best at only four stations (Fig. 4(b)). PERSIANN has the highest RMSE, with a median of 2.47. The PDF SS results show that PERSIANN and GSMaP have the highest median in regards PDF SS, followed by the ARC results. However, ARC has the lowest range, and the highest maximum and minimum, of PDF SS. Although the CHIRPS records good performance in terms of KGE and RMSE, it does not agree with the PDF of the observational data. This is shown by the low median PDF SS of CHIRPS (0.52).

Fig. 5 is a performance diagram of the five high-resolution satellite-based products. Developed by Roebber (2009), this diagram is an efficient and compact way of presenting the results of the four categorical metrics simultaneously. The x and y- axes of the diagram represent the POD and SR, respectively. The dashed lines represent the Hit BIAS (values are placed on the top and on the right axes), and the curved lines represent the CSI (values are placed on the curved lines). The optimal results are, therefore, located in the top right corner of the diagram, and the worst in the bottom left corner. It shows that the ARC and GSMaP results are significantly better than the other datasets, and TAMSAT is the worst performer. In terms of the POD, GSMaP shows the best performance (0.72) followed by ARC (0.56). Note, however, that the ARC (0.42) was slightly better than GSMaP (0.39) in terms of the SR. Both ARC and GSMaP show a similar CSI (around 0.32). Although performance of the CHIRPS product was not satisfactory, the Hit BIAS metric gives a value close to one.

#### 4.2. Evaluation of rainfall intensity categories

Fig. 6 shows the KGE of the five satellite-based rainfall products by

intensity class, on a daily scale. Fig. 7 indicates the distribution of the best performing product at each gauge locations, based on the KGE. CHIRPS records the highest median KGE under no/tiny rainfall class followed by ARC and GSMaP (Fig. 6(a)). As a result, CHIRPS appears to be the best product at the majority of the stations in Egypt, except for a few stations to the north where ARC and GSMaP have the best outcome. GSMaP, along with PERSIANN and TAMSAT, indicate very poor KGE for this category (i.e. no/tiny intensity). For the light intensity category, ARC, CHIRPS, GSMaP and TAMSAT have a KGE median in close proximity to each other (around 0.59); however, CHIRPS has the lowest variability in KGE. Due to this similarity in performance, no product could be selected as superior based on the KGE values alone (Fig. 7(b)). However, the PERSIANN is poor at replicating light intensity rainfall events. TAMSAT appears best in reproducing rainfall in the moderate-intensity class, as it has the highest median KGE ( $-0.49$ ) (Fig. 6(c)). This product appears as the best performer at more than half of the gauging stations (Fig. 7(c)). For the heavy rainfall intensity class, all five products have a very similar median KGE, but ARC exhibits a median value close to optimum ( $-0.50$ ). It should be noted that a specific pattern in the distribution of best-performing products is missing for the heavy intensity category (Fig. 7(d)).

Fig. 8 shows RMSE plots of the five satellite-based products used in reproducing daily rainfall figures in the different intensity classes. Fig. 9 shows the distribution of the best performing product at each gauge location based on the RMSE metric. For the no/tiny rainfall class, CHIRPS records the lowest RMSE (0.17 mm/day), while GSMaP and PERSIANN produce the highest median value (1.22 and 1.87 mm/day respectively). Based on these results, CHIRPS appears to be the most useful product at the majority of the gauge locations, apart from six stations located along the Mediterranean Sea where ARC appears to provide superior results (Fig. 9(a)). For the light rainfall class, all products appear to give consistent results. GSMaP has the lowest median RMSE of 2.18 mm/day and provides the best rainfall product over the sixteen gauge locations. ARC and TAMSAT appear best for five of the locations. The GSMaP product exhibits the lowest median RMSE (5.23 mm/day) when estimating moderate rainfall amounts (Fig. 8(c)), and therefore, performs best at most of the gauge locations, particularly along the Mediterranean shores (Fig. 9(c)). In the case of the heavy intensity category, all of the five products produce a similar

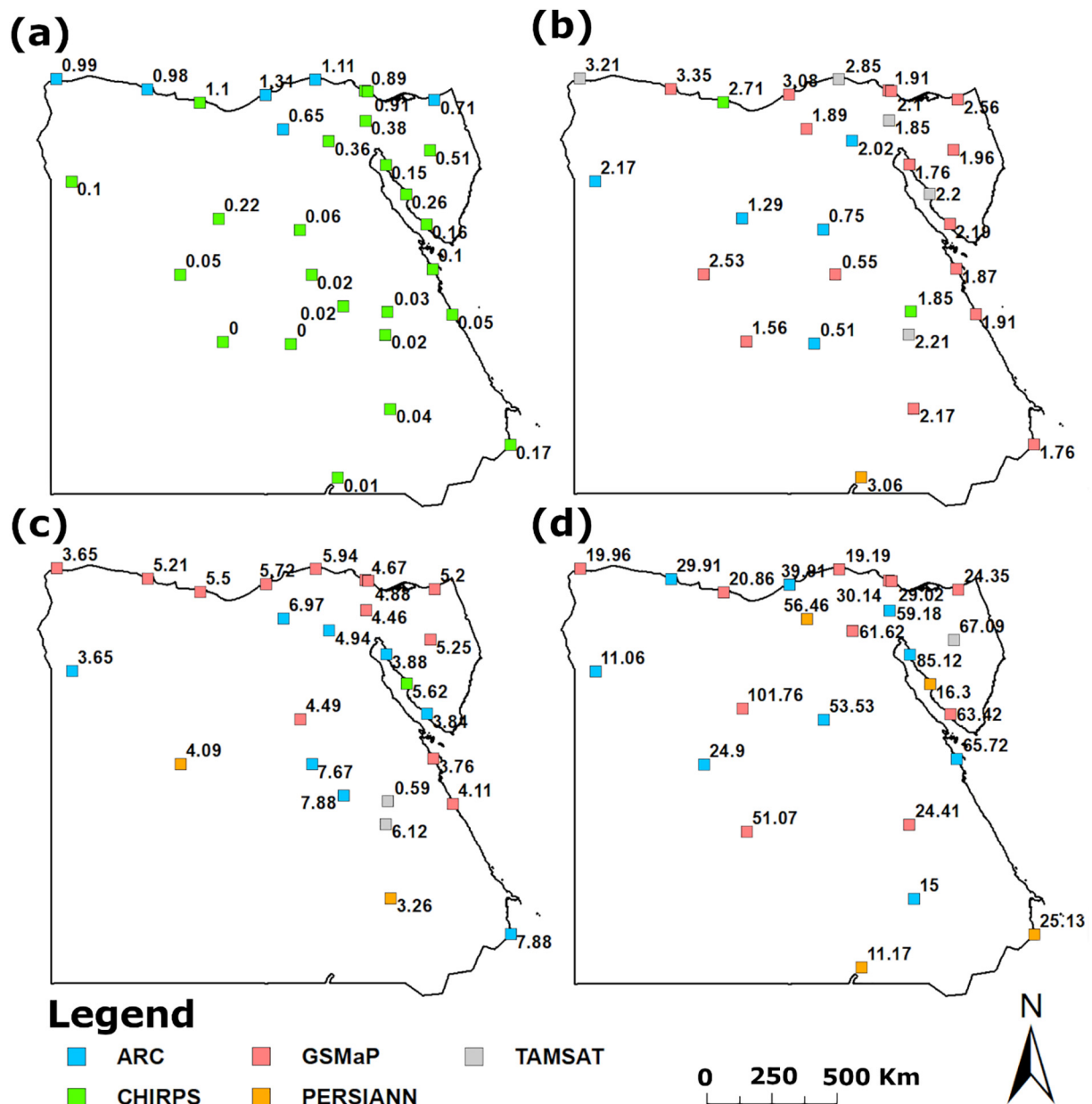


Fig. 9. Spatial distribution of the best-performing satellite precipitation products based on the RMSE for the intensity categories of: (a) no/tiny, (b) light, (c) moderate, and (d) heavy rainfall. (For interpretation of the references to colour in this figure legend, the reader is referred to the web version of this article.)

performance. However, GSMaP is best at most of the stations (11 locations), followed by the ARC product (9 locations). Overall, CHIRPS provides the best product for estimating the no/tiny rainfall class, while GSMaP exhibits the best for the light, moderate and heavy rainfall intensity categories.

The box and whisker plots of the PDF SS, replicating the rainfall total of the different rainfall intensity classes, are shown in Fig. 10. The distribution of the best performing product at each station, along with the PDF SS values, are presented in Fig. 11. In terms of the PDF SS, all the products perform poorly for all four classes. For the no/tiny class, the ARC and CHIRPS values show the highest median PDF SS (0.31 and 0.32 respectively), suggesting very good performance at most of the stations (Fig. 11(a)). For the light rainfall class, GSMaP produces the highest PDF SS median (0.56), followed by ARC (0.51). Both appear to provide the best performing products (13 for GSMaP and 7 for ARC). For the moderate and heavy rainfall categories, all the products were unable to replicate the observed PDFs. The ARC has highest median PDF SS for the moderate and high rainfall intensity classes, as shown in

Fig. 10(c-d), and therefore, performs best at most stations (Fig. 11(c-d)). Based on the PDF SS, ARC appears to provide the best result for all the rainfall intensity classes.

Fig. 12 shows the performance diagram of each rainfall product in reproducing rainy days for different daily rainfall intensity categories. Overall, the performance of the five products was better in reproducing drier days, as compared to the wetter days. All the products have a near-perfect score for detecting no/tiny rainfall days. GSMaP is best for detecting the occurrence of light rainfall events; followed by ARC. GSMaP and ARC return a similar result when reproducing moderate-intensity rainy days. GSMaP, however, produces a better score for the Hit BIAS metric. ARC is best in detecting heavy rainfall days with a POD and SR of 0.21, and a CSI slightly over 0.1. TAMSAT is the worst among the five for capturing all wet events. Overall the analyses indicate that the performance of the ARC and GSMaP methods are acceptable when reproducing rainfall days < 5 mm. However, all products seem to perform poorly in regards capturing rainfall events in other intensity categories.

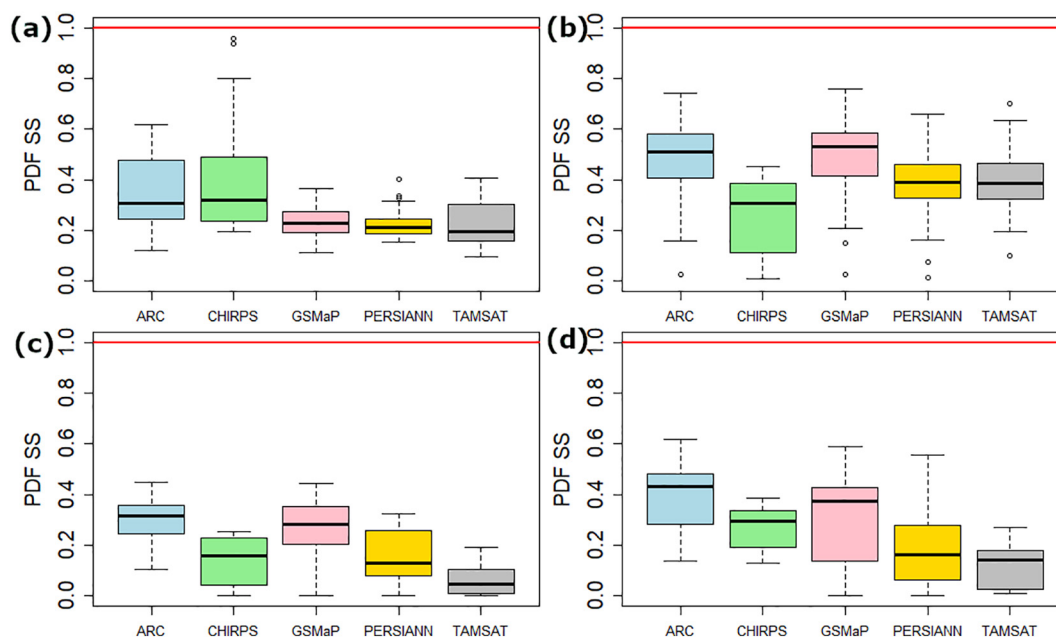


**Fig. 10.** The box and whisker plots of the PDF SS, estimated for five precipitation datasets for rainfall totals of: (a) no/tiny, (b) light, (c) moderate, and (d) heavy rainfall. The horizontal red lines represents the optimal PDF SS value.

A case study has been conducted to determine whether high resolution satellite-based gauge-corrected precipitation products could be used to reliably estimate rainfall. Most of the gauging stations in the study region had recorded rainfall on the 5th of February 2004, so the study compared the recorded rainfall amount and intensity with five satellite-based precipitation products, in order to provide further insight into the capability of these products to assist in rainfall modelling. The analysis reveals that GSMaP appears best at reliably modelling the rainfall distribution that occurred on February 5th, while CHIRPS fails to detect the heavy rainfall rate (Fig. S1). All precipitation products seem to have underestimated or overestimated the rainfall occurring on that day, as indicated in Fig. S2.

## 5. Discussion

Although all five satellite-based precipitation products performed relatively poorly when attempting to replicate the observed rainfall over the Egyptian study area, overall ARC2, CHIRPS v2.0 and GSMaP (v. 6) performed better than PERSIANN-CCS and TAMSAT (v. 3). CHIRPS showed a better KGE and RMSE, but a high FAR and low POD, and CSI in replicating the entire rainfall time-series. On the other hand, the ARC and GSMaP showed good performance in terms of the KGE, RMSE and PDF SS compared to CHIRPS. CHIRPS was very good at reproducing values for the rainfall category of < 1 mm/day, while GSMaP and ARC proved superior in estimating rainfall for light, moderate and heavy intensity events. Contingency table results indicated that ARC, CHIRPS, and GSMaP proved incapable of detecting the correct intensity category. These products also over or under-estimated the amount of rainfall for the different intensity categories. ARC and GSMaP appeared best at discriminating rainfall events of different intensities. GSMaP was the only product which provided the distribution of a relatively heavy rainfall day.

The findings of this study align with the conclusion of Nashwan et al. (2019d), that CHIRPS has the ability to estimate rainfall intensity < 1 mm. As this study was the first attempt to evaluate the remaining products (e.g. ARC v. 2, GSMaP v. 6, PERSIANN-CCS, and TAMSAT v. 3) in Egypt, it was therefore not possible to compare the performances with any previous studies. Similar research carried out in other countries with similar climatic features was selected and used for

product comparison. The work identified that both ARC and GSMaP (v. 6) overestimated recorded rainfall totals. This supports the findings of Dinku et al. (2010) over North Africa. Saber and Yilmaz (2018) found that GSMaP (v. 6) recorded a high POD (0.74) for the whole rainfall time-series in Turkey (north of Egypt) which aligns with this study finding (0.72). Dembélé and Zwart (2016) and Toté et al. (2015) also reported poor performance of ARC, CHIRPS and TAMSAT in replicating daily rainfall over Burkina Faso and Mozambique. Their observations align with the results of this study, suggesting CHIRPS is better than TAMSAT in detecting wet days. The results also align with the findings of Fenta et al. (2018), over the Lake Tana regions (Eastern Africa), where ARC performed better than CHIRPS in analyzing rainfall. However, the current results contradict with their findings in regards to the superior detection abilities of the TAMSAT product. Satellite-based precipitation products appear to perform differently in different climates and/or altitudes (Chen et al., 2018; Nashwan et al., 2018b; Saber and Yilmaz, 2018; Wu et al., 2019). Therefore, an apparent contradiction may stem from differences in climate type (or differences in the elevation of the land and the more localized climate), between Lake Tana (humid, 1800 m above sea level) and Egypt (hot desert arid, 321 m above sea level). It is worth noting that in other research, altitude has had a significant influence on the performance of satellite-based precipitation products. (Hobouchian et al., 2017).

The ARC and TAMSAT use TIR data, Meteosat First Generation Satellites 2–7 (MFG 2–7) and the Meteosat Second Generation (MSG 8–10), as their primary data source in estimating rainfall. Unlike ARC, which uses a singular threshold to compute CCDs, the TAMSAT algorithms use a spatially and temporally varying threshold to compute the CCDs. Furthermore, TAMSAT employs higher temporal resolution (15 min) TIR images, aimed at improving detection capabilities in regards short-lived rainfall events. Also, TAMSAT estimates rainfall totals using a higher resolution spatial grid ( $0.0375^\circ \times 0.0375^\circ$ ), which provides better spatial matching between gauge records and the TAMSAT data. Taking these factors into account, the performance of TAMSAT should be better than ARC, but surprisingly its performance was poorer over Egypt. Indeed, ARC homogenized the input data of the MFG 2–7 and the MSG 8–10 which has noticeable discrepancies (Novella and Thiaw, 2013). The effect of the homogenization process, however, is not noticeable in this study as homogenization was done for

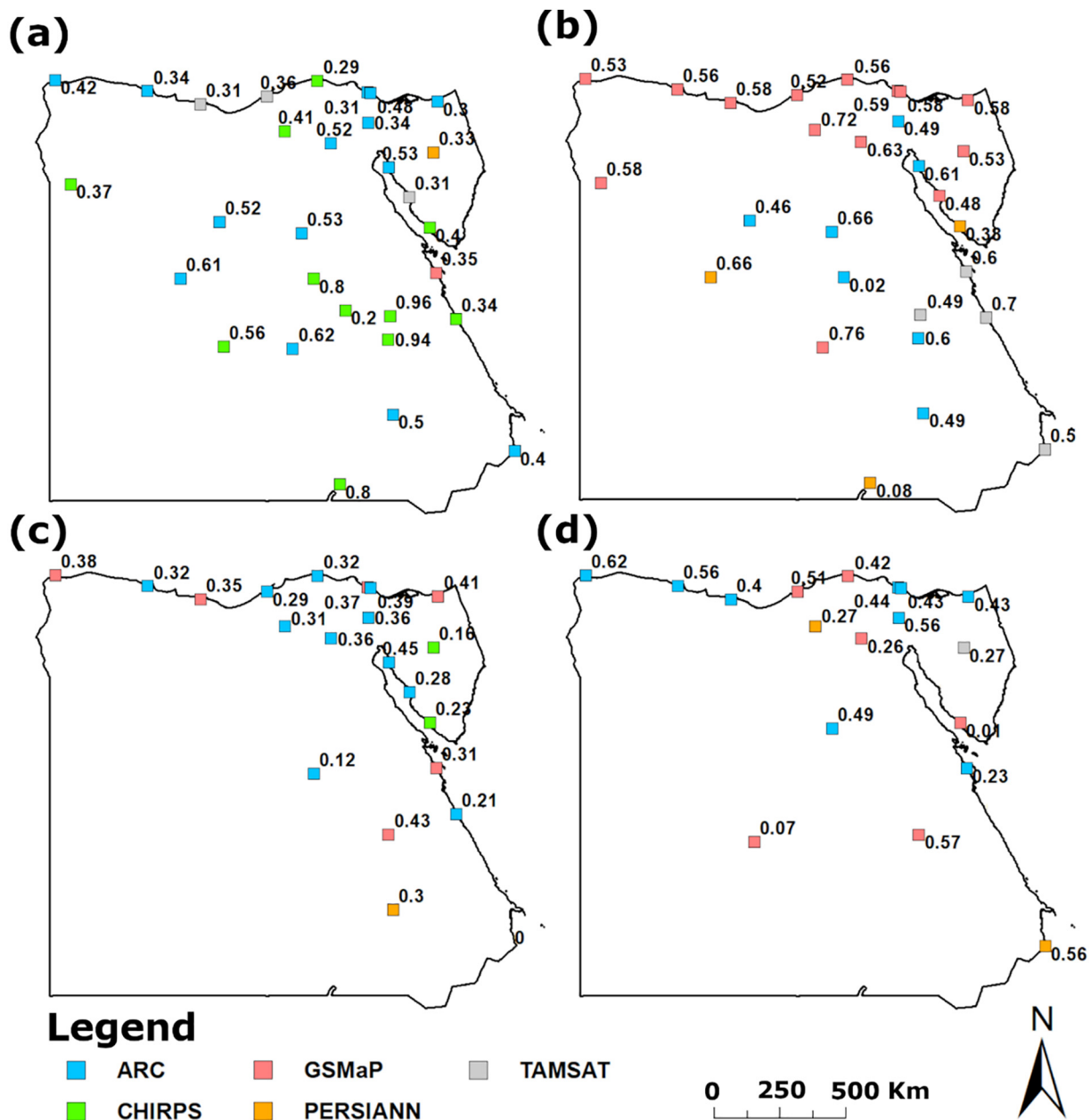


Fig. 11. Spatial distribution of the best performing precipitation product, according to the PDF SS, for the rainfall intensity categories of: (a) no/tiny, (b) light, (c) moderate, and (d) heavy rainfall. (For interpretation of the references to colour in this figure legend, the reader is referred to the web version of this article.)

the estimates from 1983 to 2005.

The poor performance of both TAMSAT and PERSIANN-CCS was noted, despite both being provided with highest resolution rainfall data. One reason for this poor performance may be due to improperly comparing gauging station records with nearest grid-based retrievals. The coarser resolution of the ARC and GSMaP data may have affected the performance of the products, in spite of the fact that fine resolution datasets such as TAMSAT and PERSIANN-CCS were expected to show superior results. This issue may be linked with the mismatch between the gauge locations and the gridded data. In addition, gauge records may not be directly correlated with the nearest satellite grid point, especially when rain propagates from the direction of another grid point. As a further line of inquiry, a comparison was made between the complete time-series of gauge data, not only to the nearest grid point of the satellite-based products, but to the other three nearest (surrounding) grid points individually, and also the mean of the nearest four (thus reducing their spatial resolution to approximately equal that

of ARC or GSMaP), using continuous statistical metrics (Sup 1). The results which indicated that neither the location of the stations nor the comparison methodology, were the issue; rather it is the actual performance of the PERSIANN-CCS and TAMSAT products over Egypt. Even though higher spatial resolution data should provide better performance when compared to coarse resolution data, the results of the current study suggest that the fine resolution data might not have acted in the way expected, at least for this arid region of Egypt. Further study is, therefore, warranted to identify the causal factors in regards this poor performance.

A major drawback in the results provided by the five satellite-based precipitation products was the overestimation of rainfall occurrence (low SR values, Fig. 5). This overestimation may be the result of three factors. The first may be the sub-cloud evaporation mechanism. The air in the lower atmosphere is very dry and hot compared to the upper air over Egypt, so despite being detected by the satellites as rainfall, any moisture may have evaporated while passing through a thick, dry and

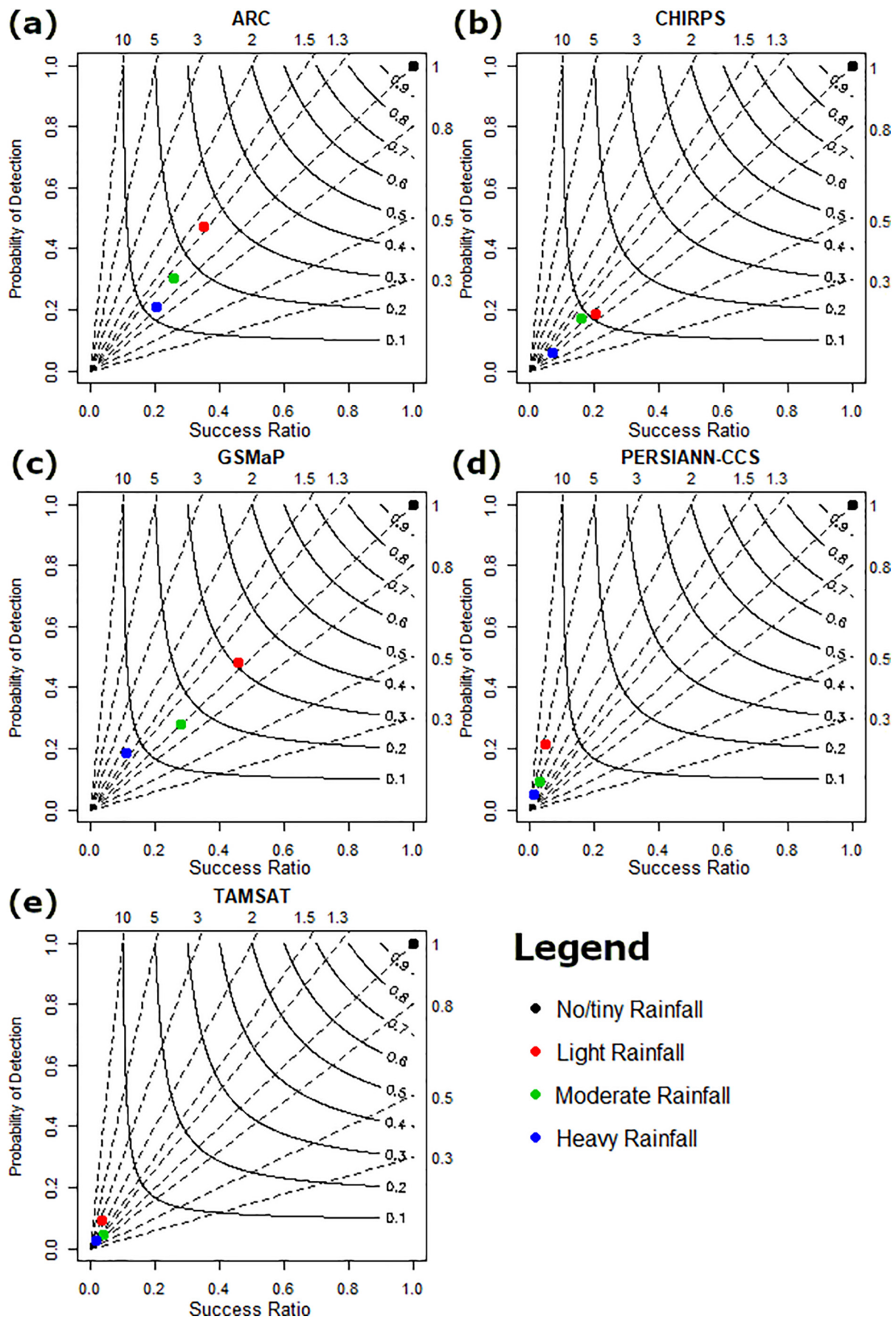


Fig. 12. Performance diagram showing the results of the categorical metrics estimated for: (a) ARC2, (b) CHIRPS v2.0, (c) GSMaP (v. 6), (d) PERSIANN-CCS, and (e) TAMSAT (v. 3). (For interpretation of the references to colour in this figure legend, the reader is referred to the web version of this article.)

hot air layer before reaching the ground stations, and so nothing was recorded (McCollum et al., 2000). The second issue could be due to the effect of the desert dust inhibiting the precipitation. Rosenfeld et al. (2001) studied the effect of desert dust of the Sahara Desert on precipitation and reported that clouds within desert dust could contain a large number of small water droplets but produce little precipitation by drop coalescence. These small droplets may not have enough velocity to overcome updrafts, and so eventually diminish rainfall. Therefore, the sand dust suppresses rainfall before it reaches the ground surface although detected as rainfall by satellite resulting in low SR. The third issue may be a result of misclassification of the surface cover by the passive microwave satellite sensors. These sensors may misidentify hot background surface and rainfall signatures, as reported in Seto et al. (2009) and Wang et al. (2009) in their works over the Sahara Desert. These three issues may combine and result in the overestimation of rainfall occurrence

## 6. Conclusion

Rainfall estimation and detection skills of five high-resolution satellite-based precipitation products were assessed using data from 30 rain gauging stations located in the hot desert region of Egypt. Seven statistical metrics and different rainfall intensity classes were used in the evaluation for the entire time-series (2003–2018). In general, the five products performed poorly. CHIRPS was best in estimating rainfall < 1 mm/day threshold. Both ARC and GSMaP were better in estimating rainfall events with a rate of > 1 mm/day and both were good in detecting rainfall. ARC was better in detecting moderate and heavy rainfall occurrences while GSMaP was better in detecting the lighter category events. Although GSMaP and ARC were regarded as good in actual rates of detection, they both suffered from a high false detection ratio. This study concluded that GSMaP may be the “best” high-resolution satellite-based precipitation product over the hot desert Egyptian domain.

As there is no dense gauging station network over Egypt, nor a high-resolution, gridded gauge-based precipitation dataset available to use for reference purposes, it was not possible to evaluate the spatial variability of rainfall retrievals by different satellite-based products.

Normally the use of several metrics is recommended for the evaluation of gridded precipitation data (Salman et al., 2018) however they often show contradictory results. This was the case in this study. Future work is warranted, including the use of information aggregation techniques (such as compromise programming (Muhammad et al., 2019; Zeleny, 1973) to integrate different metrics results into one, in order to provide more a streamlined decision-making process.

The results of this study show that despite continuous improvement in the robustness of the satellite-based precipitations products, there is room for algorithm improvement, especially over hot arid climates. The findings from this study suggest a number of further research lines of inquiry. Firstly it is unclear why the TAMSAT (v. 3) product provided a biased estimate over Egypt, despite continuous improvements in the algorithm. Secondly, more investigation is needed to identify the major reasons behind the poor performance of the PERSIANN-CCS product. Thirdly, developing a regional bias correction for GSMaP, or developing an ensemble between GSMaP and CHIRPS while preserving the extremes, would be very beneficial, especially in studies in data-scarce, gauging station-sparse countries such as Egypt. This work has provided valuable insights into the performance of different satellite-based rainfall products which may prove useful for water resource planning and management in arid regions of the world.

## Declaration of Competing Interest

The authors declare that they have no known competing financial interests or personal relationships that could have appeared to influence the work reported in this paper.

## Appendix A. Supplementary data

Supplementary data to this article can be found online at <https://doi.org/10.1016/j.atmosres.2019.104809>.

## References

- Abdallah, M.A.M., 2017. Bioaccumulation of Hydrocarbons in Freshwater fish Species Cultured in a Shallow Coastal Lagoon, Egypt. *Earth Syst. Environ.* 1, 2.
- Abdel-Fattah, M., et al., 2017. A hydrological and geomorphometric approach to understanding the generation of wadi flash floods. *Water* 9, 553.
- Abdel-Shafy, H., El-Saharty, A., Regelsberger, M., Platzer, C., 2010. Rainwater in Egypt: quantity, distribution and harvesting. *Mediterr. Mar. Sci.* 11, 245–258.
- Abutaleb, K.A.A., Mohammed, A.H.E.-S., Ahmed, M.H.M., 2018. Climate Change Impacts, Vulnerabilities and Adaption measures for Egypt's Nile Delta. *Earth Syst. Environ.* 2, 183–192.
- Abuzied, S., Yuan, M., Ibrahim, S., Kaiser, M., Saleem, T., 2016. Geospatial risk assessment of flash floods in Nuweiba area, Egypt. *J. Arid Environ.* 133, 54–72.
- Aonashi, K., et al., 2009. GSMaP passive microwave precipitation retrieval algorithm: algorithm description and validation. *J. Meteor. Soc. Jpn Ser. II (87)*, 119–136.
- Babaousmail, H., Hou, R., Ayugi, B., Gnitou, G.T., 2019. Evaluation of satellite-based precipitation estimation over Algeria during 1998–2016. *J. Atmos. Sol. Terr. Phys.* 195, 105139.
- Basheer, M., Elagib, N.A., 2019. Performance of satellite-based and GPCP 7.0 rainfall products in an extremely data-scarce country in the Nile Basin. *Atmos. Res.* 215, 128–140.
- Bayissa, Y., Tadesse, T., Demisse, G., Shiferaw, A., 2017. Evaluation of Satellite-based Rainfall estimates and Application to Monitor Meteorological Drought for the Upper Blue Nile Basin, Ethiopia. *Remote Sens.* 9, 669.
- CAPMAS, 2019. Egypt in Figures 2019 - Census March 2019 ed. Central Agency for Public Mobilization and Statistics (CAPMAS), Cairo, Egypt. pp. 16–32.
- Cattani, E., Merino, A., Guijarro, J.A., Levizzani, V., 2018. East Africa Rainfall Trends and Variability 1983–2015 using three Long-Term Satellite Products. *Remote Sens.* 10, 931.
- Chen, C., et al., 2018. Multiscale Comparative Evaluation of the GPM IMERG v5 and TRMM 3B42 v7 Precipitation Products from 2015 to 2017 over a climate transition Area of China. *Remote Sens.* 10, 944.
- Cole, D.P., Altorki, S., 1998. Bedouin, Settlers, and Holiday-Makers: Egypt's Changing Northwest Coast. *American University in Cairo Press*, Cairo, Egypt.
- Cools, J., et al., 2012. An early warning system for flash floods in hyper-arid Egypt. *Nat. Hazards Earth Syst. Sci.* 12, 443–457.
- Costa, J.E., 1987. Hydraulics and basin morphometry of the largest flash floods in the conterminous United States. *J. Hydrol.* 93, 313–338.
- Dembélé, M., Zwart, S.J., 2016. Evaluation and comparison of satellite-based rainfall products in Burkina Faso, West Africa. *Int. J. Remote Sens.* 37, 3995–4014.
- Dewan, A., Hu, K., Kamruzzaman, M., Uddin, M.R., 2019. Chapter eight - evaluating the spatiotemporal pattern of concentration, aggressiveness and seasonality of precipitation over Bangladesh with time-series Tropical Rainfall measuring Mission data. In: Maggioni, V., Massari, C. (Eds.), *Extreme Hydroclimatic Events and Multivariate Hazards in a Changing Environment*, Elsevier, pp. 191–219.
- Dinku, T., Ceccato, P., Cressman, K., Connor, S.J., 2010. Evaluating Detection skills of Satellite Rainfall estimates over Desert Locust recession Regions. *J. Appl. Meteorol. Climatol.* 49, 1322–1332.
- El Bastawesy, M., White, K., Nasr, A., 2009. Integration of remote sensing and GIS for modelling flash floods in Wadi Hudain catchment, Egypt. *Hydrol. Process. Int. J.* 23, 1359–1368.
- El Kenawy, A.M., et al., 2019. Spatial assessment of the performance of multiple high-resolution satellite-based precipitation data sets over the Middle East. *Int. J. Climatol.* 39, 2522–2543.
- El-Magd, I.A., Hermas, E., El Bastawesy, M., 2010. GIS-modelling of the spatial variability of flash flood hazard in Abu Dabbab catchment, Red Sea Region, Egypt. *Egypt. J. Remote Sens. Space Sci.* 13, 81–88.
- Fenta, A.A., et al., 2018. Evaluation of satellite rainfall estimates over the Lake Tana basin at the source region of the Blue Nile River. *Atmos. Res.* 212, 43–53.
- FloodList, 2015. Egypt – floods in alexandria leave at least. In: *Dead. FLOODLIST NEWS, FloodList.* 6.
- FloodList, 2018. Eastern Mediterranean – Deadly Flash Floods after Heavy Rain. *FLOODLIST NEWS, FloodList.*
- Funk, C., et al., 2015. The climate hazards infrared precipitation with stations—a new environmental record for monitoring extremes. *Scientific Data* 2, 150066.
- Gado, T.A., El-Agha, D.E., 2019. Feasibility of rainwater harvesting for sustainable water management in urban areas of Egypt. *Environ. Sci. Pollut. Res.* 1–14.
- Gado, T.A., El-Hagsry, R.M., Rashwan, I.M.H., 2019. Spatial and temporal rainfall changes in Egypt. *Environ. Sci. Pollut. Res.* 26, 28228–28242.
- Gella, G.W., 2019. Statistical evaluation of High Resolution satellite precipitation products in arid and semi-arid parts of Ethiopia: a note for hydro-meteorological applications. *Water Environ. J.* 33, 86–97.
- Gupta, H.V., Kling, H., Yilmaz, K.K., Martinez, G.F., 2009. Decomposition of the mean squared error and NSE performance criteria: Implications for improving hydrological modelling. *J. Hydrol.* 377, 80–91.
- Hamed, K.H., 2019. Stochastic Investigation of the GERD-AHD Interaction through first Impoundment and beyond. In: Negm, A.M., Abdel-Fattah, S. (Eds.), *Grand Ethiopian Renaissance Dam Versus Aswan High Dam: A View from Egypt*. Springer International Publishing, Cham, pp. 95–117.

- Hobouchian, M.P., Salio, P., García Skabar, Y., Vila, D., Garreaud, R., 2017. Assessment of satellite precipitation estimates over the slopes of the subtropical Andes. *Atmos. Res.* 190, 43–54.
- Hong, Y., Hsu, K.-L., Sorooshian, S., Gao, X., 2004. Precipitation estimation from remotely sensed imagery using an artificial neural network cloud classification system. *J. Appl. Meteorol.* 43, 1834–1853.
- Huffman, G.J., et al., 2001. Global Precipitation at One-Degree Daily Resolution from Multisatellite Observations. *J. Hydrometeorol.* 2, 36–50.
- Katsanos, D., Retalis, A., Michaelides, S., 2016. Validation of a high-resolution precipitation database (CHIRPS) over Cyprus for a 30-year period. *Atmos. Res.* 169, 459–464.
- Krichak, S.O., Tsidulko, M., Alpert, P., 2000. November 2, 1994, severe storms in the southeastern Mediterranean. *Atmos. Res.* 53, 45–62.
- Levizzani, V., Cattani, E., 2019. Satellite Remote Sensing of Precipitation and the Terrestrial Water Cycle in a changing climate. *Remote Sens.* 11, 2301.
- Llasat, M.C., et al., 2010. High-impact floods and flash floods in Mediterranean countries: the FLASH preliminary database. *Adv. Geosci.* 23, 47–55.
- Mahrooghy, M., Anantharaj, V.G., Younan, N.H., Aanstoos, J., Hsu, K.-L., 2012. On an Enhanced PERSIANN-CCS Algorithm for Precipitation Estimation. *J. Atmos. Ocean. Technol.* 29, 922–932.
- Maidment, R.I., et al., 2017. A new, long-term daily satellite-based rainfall dataset for operational monitoring in Africa. *Scientific Data* 4, 170063.
- Mashaly, J., Ghoneim, E., 2018. Flash flood hazard using optical, radar, and stereo-pair derived DEM: Eastern Desert, Egypt. *Remote Sens.* 10, 1204.
- McCollum, J.R., Gruber, A., Ba, M.B., 2000. Discrepancy between Gauges and Satellite estimates of Rainfall in Equatorial Africa. *J. Appl. Meteorol.* 39, 666–679.
- Mega, T., et al., 2014. Gauge adjusted global satellite mapping of precipitation (GSMaP\_Gauge). *General Assembly and Scientific Symposium (URSI GASS), 2014 XXXIth URSI.* IEEE 1–4.
- Muhammad, M.K.I., et al., 2019. Evaluation of empirical reference evapotranspiration models using compromise programming: a case study of Peninsular Malaysia. *Sustainability* 11, 4267.
- Nashwan, M.S., Shahid, S., 2019a. Spatial distribution of unidirectional trends in climate and weather extremes in Nile river basin. *Theor. Appl. Climatol.* 137, 1181–1199.
- Nashwan, M.S., Shahid, S., 2019b. Symmetrical uncertainty and random forest for the evaluation of gridded precipitation and temperature data. *Atmos. Res.* 230, 104632.
- Nashwan, M.S., Ismail, T., Ahmed, K., 2018a. Flood susceptibility assessment in Kelantan river basin using copula. *Int. J. Eng. Technol.* 7, 584–590.
- Nashwan, M.S., Shahid, S., Chung, E.-S., Ahmed, K., Song, Y.H., 2018b. Development of Climate-based Index for Hydrologic Hazard Susceptibility. *Sustainability* 10, 2182.
- Nashwan, M.S., Ismail, T., Ahmed, K., 2019a. Non-stationary analysis of extreme rainfall in Peninsular Malaysia. *J. Sustain. Sci. Manag.* 14, 17–34.
- Nashwan, M.S., Shahid, S., Abd Rahim, N., 2019b. Unidirectional trends in annual and seasonal climate and extremes in Egypt. *Theor. Appl. Climatol.* 136, 457–473.
- Nashwan, M.S., Shahid, S., Chung, E.-S., 2019c. Development of high-resolution daily gridded temperature datasets for the central north region of Egypt. *Scientific Data* 6, 138.
- Nashwan, M.S., Shahid, S., Wang, X.-J., 2019d. Assessment of satellite-based precipitation measurement products over the hot desert climate of Egypt. *Remote Sens.* 11, 555.
- Nashwan, M.S., Shahid, S., Wang, X.-J., 2019e. Uncertainty in estimated trends using gridded rainfall data: a case study of Bangladesh. *Water* 11, 349.
- Nikolopoulos, E.I., Anagnostou, E.N., Borga, M., 2013. Using High-Resolution Satellite Rainfall Products to Simulate a Major Flash Flood Event in Northern Italy. *J. Hydrometeorol.* 14, 171–185.
- Novella, N.S., Thiaw, W.M., 2013. African rainfall climatology version 2 for famine early warning systems. *J. Appl. Meteorol. Climatol.* 52, 588–606.
- OGIMET, 2018. SYNOP of Cairo Airport (Egypt) on 04/25/2018 at 00:00 UTC.
- Perkins, S.E., Pitman, A.J., Holbrook, N.J., McAneney, J., 2007. Evaluation of the AR4 climate Models' simulated Daily Maximum Temperature, Minimum Temperature, and Precipitation over Australia using Probability Density Functions. *J. Clim.* 20, 4356–4376.
- Petersen, W.A., Christian, H.J., Rutledge, S.A., 2005. TRMM observations of the global relationship between ice water content and lightning. *Geophys. Res. Lett.* 32.
- Roebber, P.J., 2009. Visualizing Multiple measures of Forecast Quality. *Weather Forecast.* 24, 601–608.
- Rosenfeld, D., Rudich, Y., Lahav, R., 2001. Desert dust suppressing precipitation: a possible desertification feedback loop. *Proc. Natl. Acad. Sci.* 98, 5975.
- Rozante, J., Vila, D., Barboza Chiquetto, J., Fernandes, A., Souza Alvim, D., 2018. Evaluation of TRMM/GPM Blended Daily Products over Brazil. *Remote Sens.* 10, 882.
- Saber, M., Yilmaz, K.K., 2018. Evaluation and bias correction of satellite-based rainfall estimates for modelling flash floods over the mediterranean region: application to Karpuz River Basin, Turkey. *Water* 10, 657.
- Salman, S.A., Shahid, S., Ismail, T., Ahmed, K., Wang, X.-J., 2018. Selection of climate models for projection of spatiotemporal changes in temperature of Iraq with uncertainties. *Atmos. Res.* 213, 509–522.
- Salman, S.A., et al., 2019. Selection of gridded precipitation data for Iraq using compromise programming. *Measurement* 132, 87–98.
- Seto, S., Kubota, T., Iguchi, T., Takahashi, N., Oki, T., 2009. An evaluation of over-land rain rate estimates by the GSMaP and GPROF algorithms: the role of lower-frequency channels. *J. Meteor. Soc. Jpn Ser. II* 87A, 183–202.
- Smith, B., Rodriguez, S., 2017. Spatial analysis of high-resolution radar rainfall and citizen-reported flash flood data in ultra-urban New York City. *Water* 9, 736.
- Stanley, D.J., Warne, A.G., 1993. Nile Delta: recent geological evolution and human impact. *Science* 260, 628–634.
- Toté, C., et al., 2015. Evaluation of Satellite Rainfall estimates for Drought and Flood monitoring in Mozambique. *Remote Sens.* 7, 1758–1776.
- Trejo, F.J.P., Barbosa, H.A., Peñaloza-Murillo, M.A., Alejandra Moreno, M., Farías, A., 2016. Intercomparison of improved satellite rainfall estimation with CHIRPS gridded product and rain gauge data over Venezuela. *Atmósfera* 29, 323–342.
- Ushio, T., et al., 2009. A Kalman filter approach to the Global Satellite Mapping of Precipitation (GSMaP) from combined passive microwave and infrared radiometric data. *J. Meteor. Soc. Jpn Ser. II* (87), 137–151.
- Wang, N.-Y., et al., 2009. TRMM 2A12 Land Precipitation Product - Status and Future Plans. *J. Meteor. Soc. Jpn Ser. II* 87A, 237–253.
- WMO, 2012. Observation of present and past weather; state of the ground. In: *Guide to Meteorological Instruments and Methods of Observation.* 14–19. WMO, Geneva, Switzerland, pp. I.
- Wu, Y., et al., 2019. Evaluation of the GPM IMERG v5 and TRMM 3B42 v7 Precipitation Products in the Yangtze River Basin, China. *Water* 11, 1459.
- Youssef, A.M., Pradhan, B., Hassan, A.M., 2011. Flash flood risk estimation along the St. Katherine road, southern Sinai, Egypt using GIS based morphometry and satellite imagery. *Environ. Earth Sci.* 62, 611–623.
- Zeleny, M., 1973. *Compromise Programming, Multiple Criteria Decision-making.* University of South Carolina Press, Columbia, pp. 263–301.